Journal of the Korean Physical Society, Vol. 48, February 2006, pp. S152∼S156

Eigenvalue-Matching Renormalization-Group Analysis of Tricritical Behavior in Unidirectionally Coupled Maps

Woochang LIM* and Sang-Yoon KIM†

Department of Physics, Kangwon National University, Chunchon 200-701

We study the scaling behavior in two unidirectionally coupled one-dimensional maps near tricritical points which lie at ends of Feigenbaum critical lines and near edges of the complicated parts of the boundary of chaos. Note that both period-doubling cascades to chaos and multistability (associated with saddle-node bifurcations) occur in any neighborhood of the tricritical point. For this tricritical case, the response subsystem exhibits a type of non-Feigenbaum codimension-2 scaling behavior, while the drive subsystem is in a periodic state. To analyze the tricritical behavior, we develop an eigenvalue-matching renormalization-group (RG) method and obtain the scaling factors. These RG results agree well with those of previous work.

PACS numbers: 05.45.Jn
Keywords: Unidirectionally coupled maps, Tricritical behavior, Eigenvalue-matching renormalization-group analysis

I. INTRODUCTION

Transition to chaos *via* period doublings has been extensively studied in a one-parameter family of one-dimensional (1D) unimodal maps with a quadratic extremum. As a control parameter is increased, the 1D map exhibits an infinite sequence of period-doubling bifurcations accumulating at a critical point, beyond which chaos sets in. Feigenbaum [1] developed a renormalization-group (RG) method and discovered universal scaling behavior near the critical point. This work has been generalized to two-parameter families of 1D bimodal maps with two extrema [2]. The boundary of chaos in the parameter plane consists of the Feigenbaum critical lines and a Cantor-like set of critical points. The simplest representative among the codimension-two critical points is a tricritical point which is just an end of a Feigenbaum critical line. A (non-Feigenbaum) two-parameter scaling has been found near the tricritical points in the two-parameter family of 1D quartic maps [3]. Extension of this tricriticality to multidimensional invertible systems has also been discussed [4].

In this paper, we study the tricritical behavior in a system consisting of two 1D maps with a one-way coupling,

$$x_{t+1} = 1 - Ax_t^2, \quad y_{t+1} = 1 - By_t^2 - Cx_t^2, \tag{1}$$

where x and y are state variables of the first and second subsystems, A and B are control parameters of the subsystems, and C is a coupling parameter. Note that the first (drive) subsystem acts on the second (response) subsystem, while the second subsystem does not influence the first subsystem. Recently, these unidirectionally coupled systems have been actively discussed in application to secure communication using chaos synchronization [5]. For a fixed value of C, a kind of non-Feigenbaum scaling behavior appears near a bicritical point where two Feigenbaum critical lines of the drive and response subsystems meet. This bicritical case has been extensively investigated [6, 7]. Here, we are interested in another kind of non-Feigenbaum scaling behavior. When the first drive system is in a periodically oscillating state for some given A, the second response subsystem has been found to exhibit a tricritical scaling behavior as in the case of 1D bimodal maps [8]. We develop an eigenvalue-matching RG method [9] for the tricriticality and obtain the scaling factors.

This paper is organized as follows. In Section II we recapitulate the tricritical behavior of the response subsystem in two unidirectionally coupled 1D maps when the drive system is in a period-4 state for $A = 1.3$. Similar to the case of the 1D bimodal maps, there exist doubly superstable periodic orbits containing two critical points where the Jacobian determinant of the unidirectionally coupled maps becomes zero. The set of doubly superstable points in the $B-C$ parameter plane may be organized into a binary tree. A specific route in this tree, which ends in an infinite number of left or right steps, leads to a tricritical point which is just an end of a Feigenbaum critical line. The scaling behavior near the tricritical point is confirmed by showing repeated self-similar structures in the state diagram. In the main Section III, we employ an "eigenvalue-matching" RG method, equat-

*E-mail: wclim@kangwon.ac.kr;
†Corresponding Author: sykim@kangwon.ac.kr

ing the successive three stability multipliers of the orbits of level n (period 2^n), $n+1$, and $n+2$, and make the RG analysis of the tricritical behavior. Thus, we numerically obtain the tricritical point, the parameter and orbital scaling factors, and the critical stability multiplier. We note that the accuracy is improved remarkably on increasing the level n and the results agree well with those of previous work [2–4,8]. Finally, a summary is given in Section IV.

II. SCALING BEHAVIOR NEAR A TRICRITICAL POINT

In this section, we recapitulate the tricritical behavior in the two unidirectionally coupled 1D maps of Eq. (1) for $A = 1.3$. Near a tricritical point, the response subsystem is shown to exhibit a (non-Feigenbaum) two-parameter scaling in the $B-C$ parameter plane.

Stability of an orbit with period q in the two unidirectionally coupled 1D maps is determined by its stability multipliers,

$$\lambda_1 = \prod_{t=1}^{q}(-2Ax_t), \quad \lambda_2 = \prod_{t=1}^{q}(-2By_t). \tag{2}$$

Here, λ_1 and λ_2 determine the stability of the first and second subsystems, respectively. An orbit becomes stable when the moduli of both multipliers are less than unity, *i.e.*,$-1 < \lambda_i < 1$ for $i = 1, 2$. For $A = 1.3$, the (first) drive subsystem is in a period-4 state with $\lambda_1 = 0.180\,542\cdots$, $x_0(= -0.014\,946\cdots) \rightarrow x_1(= 0.999\,709\cdots) \rightarrow x_2(= -0.299\,245\cdots) \rightarrow x_3(= 0.883\,588\cdots) \rightarrow x_4(= x_0)$. On the other hand, the (second) response subsystem exhibits rich dynamical behaviors, depending on the values of B and C.

Figure 1(a) shows bifurcation curves of the response subsystem in the $B-C$ plane. The bifurcation pattern contains "swallow" structures, as in the 1D bimodal maps [10]. We start from the basic period 4. When passing the D_4 black curve, the period-4 state becomes unstable through a period-doubling bifurcation (*i.e.*, $\lambda_2 = -1$ curve), and then a stable period-8 state appears in the response subsystem. It is numerically found that a periodic orbit may become superstable when it contains a critical point, $z_L = (x_L, 0)$ or $z_R = (x_R, 0)$, where $x_L[\equiv x_0(= -0.014\,946\cdots)]$ and $x_R[\equiv x_3(= 0.883\,588\cdots)]$. For this supercritical case, the 2nd stability multiplier of the periodic orbit becomes zero (*i.e.*, $\lambda_2 = 0$). Inside the D_4 curve, there exist two superstable gray curves 8_L and 8_R, on which the period-8 orbit becomes superstable because it contains z_L and z_R, respectively. These 8_L and 8_R curves cross twice, forming a loop, at the lower doubly superstable point (denoted by a circle) and at the upper bistability point (denoted by a plus). At the doubly superstable point, the period-8 orbit becomes doubly superstable because it contains both the critical points, z_L and z_R. On the other hand, there exist two independent superstable period-8 orbits at the bistability point. This bistability arises from a cusp catastrophe within the loop. At the cusp (denoted by a cross), a pair of saddle-node bifurcation curves S_8 (shown in dark gray), giving rise to a pair of stable and unstable period-8 orbits, meet. In addition to the S_8 curves, there exist two period-doubling bifurcation curves D_8 in the period-8 zone. These D_8 curves cross once just above the cusp, and they move from one superstable curve to another one in going from an outer period-doubling prong to an inner saddle-node prong. Thus, inside the period-8 zone, two superstable curves 8_L and 8_R, two D_8 curves, and two S_8 curves form a swallow-shaped area. Two similar, smaller, swallow-shaped areas appear inside the D_8 curves of the next higher level (*i.e.*, in the period-16 zone). In this way, since the number of swallow-shaped areas doubles with each period doubling, a Cantor-like set of cusps and the

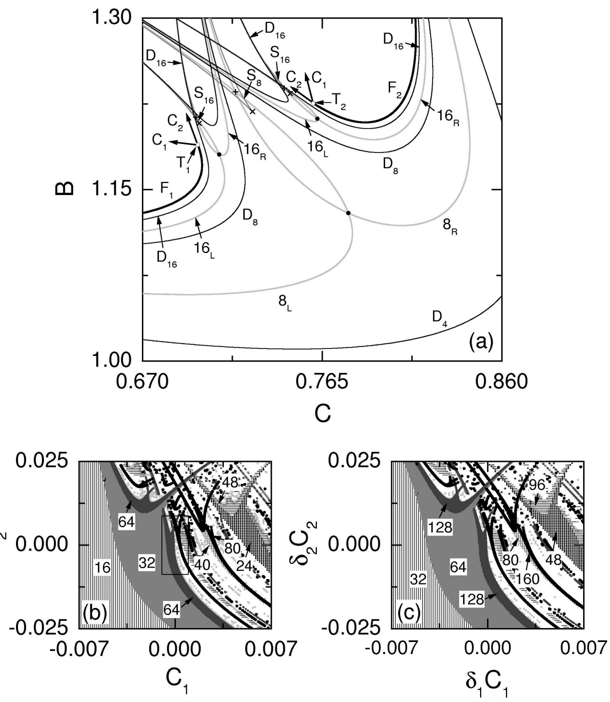

Fig. 1. (a) Swallow-shaped structure of bifurcation curves of the response subsystem in the $B-C$ plane for $A = 1.3$. There are two superstable curves of the period-q orbit denoted by the q_L and q_R gray curves. In addition to them, black lines D_q and dark gray lines S_q represent the period-doubling and saddle-node bifurcation curves of the q-periodic orbit, respectively. (b) and (c) Self-similar topography of the parameter plane near the tricritical point T_1 in the C_1-C_2 plane (C_1 and C_2 are scaling coordinates representing eigendirections). The numbers denote periods of dynamical states, and chaos or higher periodic states are represented in white. Magnification of the small box in (b) along the C_1 and C_2 axes by the factors δ_1 and δ_2 reproduces the same topography of the parameter plane. For more details, see the text.

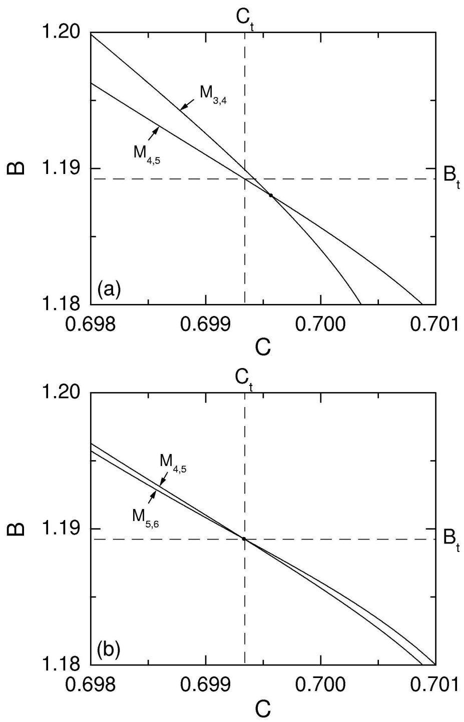

Fig. 2. Plots of the $M_{n,n+1}$ curve at which $\lambda_{2,n} = \lambda_{2,n+1}$ in the $B-C$ plane for $A = 1.3$. In (a) the intersection point of the two curves, denoted by a solid circle, gives the tricritical point (B_3^*, C_3^*) of level 3. (b) As the level n is increased, (B_n^*, C_n^*) approaches the tricritical point $(B_t, C_t) = (1.189\,249\cdots, 0.699\,339\cdots)$. For more details, see the text.

associated superstable crossings (*i.e.* bistability points and doubly superstable points) may be organized into an infinite binary tree coded by two symbols (*e.g.*, "L" and "R").

Following a specific route with code $[(L,)^\infty] = [L, L, L, \cdots]$ or $[(R,)^\infty] = [R, R, R, \cdots]$ in the binary tree, we reach a tricritical point T_1 with $(B_t, C_t) = (1.189\,249\cdots, 0.699\,339\cdots)$ or T_2 with $(B_t, C_t) = (1.225\,396\cdots, 0.760\,267\cdots)$. Two-parameter scaling occurs near each tricritical point as follows [3]. An infinite sequence of doubly superstable points converge geometrically to the tricritical point with the scaling factor $\delta_1 (= 7.284\,685)$ along the scaling axis C_1. On the other hand, an infinite sequence of bistability points or cusps accumulates to the tricritical point with the scaling factor δ_2 $(= 2.857\,124)$ along the scaling axis C_2 (but from the opposite side). To demonstrate this scaling near T_1, we first introduce scaling coordinates C_1 and C_2 such that $\Delta B (\equiv B - B_t) = 0.60 C_1 + 0.97 C_2$ and $\Delta C (\equiv C - C_t) = -0.79 C_1 - 0.22 C_2$. Figure 1(b) shows rich dynamical states near T_1 in the $C_1 - C_2$ plane. Here the tricritical point T_1 is located exactly at the origin, the numbers denote periods of dynamical states, and chaos or very high periodic states are denoted in white. As shown in Figure 1(c), the topography of the parameter plane is reproduced by magnifying a small box in Figure 1(b) along the scaling axes C_1 and C_2 by the factors δ_1 and δ_2.

III. EIGENVALUE-MATCHING RG ANALYSIS OF THE TRICRITICAL BEHAVIOR

In this section, we employ an eigenvalue-matching RG method and make the RG analysis of the scaling behavior of the response subsystem near the tricritical point T_1 in the two unidirectionally coupled 1D maps for $A = 1.3$. The recurrence relations of the old parameters (B, C) and the new (renormalized) parameters (B', C') are given by equating the second stability multipliers of the successive three orbits of level n (period 2^n), $n+1$, and $n+2$, *i.e.*,

$$\lambda_{2,n}(B, C) = \lambda_{2,n+1}(B', C'), \tag{3a}$$

$$\lambda_{2,n+1}(B, C) = \lambda_{2,n+2}(B', C'). \tag{3b}$$

Here $\lambda_{2,n}$ is the second stability multiplier of the orbit with period 2^n.

The fixed point (B_n^*, C_n^*) of the renormalization transformation (3) of level n,

$$\lambda_{2,n}(B_n^*, C_n^*) = \lambda_{2,n+1}(B_n^*, C_n^*), \tag{4a}$$

$$\lambda_{2,n+1}(B_n^*, C_n^*) = \lambda_{2,n+2}(B_n^*, C_n^*) \tag{4b}$$

approaches the tricritical point $(B_t, C_t) = (1.189\,249\cdots, 0.699\,339\cdots)$ as $n \to \infty$. Linearizing the renormalization transformation (3) at the fixed point (B_n^*, C_n^*), we obtain

$$\begin{pmatrix} \Delta B \\ \Delta C \end{pmatrix} = \begin{pmatrix} \frac{\partial B}{\partial B'}\Big|_* & \frac{\partial B}{\partial C'}\Big|_* \\ \frac{\partial C}{\partial B'}\Big|_* & \frac{\partial C}{\partial C'}\Big|_* \end{pmatrix} \begin{pmatrix} \Delta B' \\ \Delta C' \end{pmatrix} \tag{5a}$$

$$= \Delta_n \begin{pmatrix} \Delta B' \\ \Delta C' \end{pmatrix}, \tag{5b}$$

where $\Delta B = B - B_n^*$, $\Delta C = C - C_n^*$, $\Delta B' = B' - B_n^*$, $\Delta C' = C' - C_n^*$, and

$$\Delta_n = \Gamma_n^{-1} \Gamma_{n+1}, \tag{6a}$$

$$\Gamma_n = \begin{pmatrix} \frac{\partial \lambda_{2,n}}{\partial B}\Big|_* & \frac{\partial \lambda_{2,n}}{\partial C}\Big|_* \\ \frac{\partial \lambda_{2,n+1}}{\partial B}\Big|_* & \frac{\partial \lambda_{2,n+1}}{\partial C}\Big|_* \end{pmatrix}, \tag{6b}$$

$$\Gamma_{n+1} = \begin{pmatrix} \frac{\partial \lambda_{2,n+1}}{\partial B'}\Big|_* & \frac{\partial \lambda_{2,n+1}}{\partial C'}\Big|_* \\ \frac{\partial \lambda_{2,n+2}}{\partial B'}\Big|_* & \frac{\partial \lambda_{2,n+2}}{\partial C'}\Big|_* \end{pmatrix}. \tag{6c}$$

(Here Γ_n^{-1} is the inverse of Γ_n.) As $n \to \infty$, the eigenvalues $\delta_{1,n}$ and $\delta_{2,n}$ of the matrix Δ_n converge to δ_1 $(= 7.284\,69)$ and δ_2 $(= 2.857\,12)$, which are just the parameter scaling factors for the response subsystem. Furthermore, the local rescaling factor of the state variable y of the response subsystem in the most rarified region is simply given by

$$\alpha_n = \frac{y_n - y_{n+1}}{y_{n+1} - y_{n+2}} \quad \text{for } (B, C) = (B_n^*, C_n^*), \tag{7}$$

Table 1. Sequences of the tricritical point and the critical second stability multiplier, $\{B_n^*\}$, $\{C_n^*\}$, and $\{\lambda_{2,n}^*\}$.

n	B_n^*	C_n^*	$\lambda_{2,n}^*$
3	1.188 031 357 461	0.699 568 017 742	-2.004 916
4	1.189 278 323 347	0.699 332 962 713	-2.052 459
5	1.189 241 876 101	0.699 340 786 906	-2.048 510
6	1.189 249 350 331	0.699 339 111 107	-2.050 806
7	1.189 249 318 839	0.699 339 118 284	-2.050 779
8	1.189 249 375 785	0.699 339 105 224	-2.050 921
9	1.189 249 376 834	0.699 339 104 983	-2.050 928
10	1.189 249 377 334	0.699 339 104 868	-2.050 939
11	1.189 249 377 352	0.699 339 104 863	-2.050 940
12	1.189 249 377 357	0.699 339 104 862	-2.050 940
13	1.189 249 377 357	0.699 339 104 862	-2.050 940
14	1.189 249 377 357	0.699 339 104 862	-2.050 940

Table 2. Sequences of the parameter and orbital scaling factors, $\{\delta_{1,n}\}$, $\{\delta_{2,n}\}$, and $\{\alpha_n\}$.

n	$\delta_{1,n}$	$\delta_{2,n}$	α_n
3	6.389 726	3.064 274	-1.772 564
4	7.378 722	2.834 330	-1.708 159
5	7.243 372	2.866 203	-1.700 798
6	7.286 477	2.856 633	-1.693 945
7	7.282 234	2.857 639	-1.691 796
8	7.284 642	2.857 130	-1.690 845
9	7.284 515	2.857 159	-1.690 508
10	7.284 674	2.857 126	-1.690 377
11	7.284 673	2.857 127	-1.690 330
12	7.284 684	2.857 124	-1.690 313
13	7.284 685	2.857 124	-1.690 306
14	7.284 685	2.857 124	-1.690 304

where y_n is the orbit point with largest distance from its nearest orbit point in the 2^n-periodic orbit of the response subsystem. Here, α_n also converge to the orbital scaling factor α ($= -1.690\,30$) of the response subsystem, as n goes to infinity.

Some results in the low orders are shown in Figure 2(a) and (b). Figure 2(a) shows two curves $M_{3,4}$ (where $\lambda_{2,3} = \lambda_{2,4}$) and $M_{4,5}$ (where $\lambda_{2,4} = \lambda_{2,5}$) in the $B - C$ plane. We note that the intersection point, denoted by the solid circle, of the two curves gives the tricritical point (B_3^*, C_3^*) of level 3, at which the value of the second stability multiplier $(\lambda_{2,3}^*)$ is just the critical second stability multiplier of level 3. On increasing the level n, (B_n^*, C_n^*) becomes closer to the tricritical point $(B_t, C_t) = (1.189\,249\cdots, 0.699\,339\cdots)$, as shown in Figure 2(b). Eventually, (B_n^*, C_n^*) and $\lambda_{2,n}^*$ converge to the tricritical point (B_t, C_t) and the critical second stability multiplier λ_2^* ($= -2.050\,940$) (which is just the limit value of the second stability multipliers of 2^n-periodic orbits at the tricritical point), respectively.

Increasing the level up to $n = 14$, we numerically make the RG analysis of the tricritical scaling behavior. We first solve Eq. (4) and obtain the tricritical point (B_n^*, C_n^*) of level n and the critical second stability multiplier $(\lambda_{1,n}^*, \lambda_{2,n}^*)$ of level n. The results are listed in Table 1. Next, we obtain the parameter scaling factors $\delta_{1,n}$ and $\delta_{2,n}$ from the eigenvalues of Δ_n in Eq. (6a) and the orbital scaling factor α_n from Eq. (7). These results are listed in Table 2. Note that the accuracy in the numerical RG results is remarkably improved with the level n and their limit values agree well with those obtained in previous work.

IV. SUMMARY

We have studied the scaling behavior near a tricritical point in two unidirectionally coupled 1D maps. For this tricritical case, the response subsystem exhibits a (non-Feigenbaum) two-parameter scaling behavior, while the drive subsystem is in a periodic state. To make the RG analysis of this tricritical behavior, we have employed an eigenvalue-matching method and obtained the bicritical point, the parameter and orbital scaling factors, and the critical stability multiplier. Note that the numerical accuracy in the RG results is improved remarkably on increasing the order n. Consequently, these RG results agree well with the results of previous work.

REFERENCES

[1] M. J. Feigenbaum, J. Stat. Phys. **19**, 25 (1978); bidi **21**, 669 (1979).

[2] S. Fraser and R. Kapral, Phys. Rev. A **30**, 107 (1984); R. S. MacKay and J. B. J. van Zeijts, Nonlinearity **1**, 253 (1988).

[3] S.-J. Chang, M. Wortis and J. A. Wright, Phys. Rev. A **24**, 2669 (1981).

[4] S. P. Kuznetsov, Phys. Lett. A **169**, 438 (1992); A. P. Kuznetsov, S. P. Kuznetsov and I. R. Sataev, Phys. Lett. A **184**, 413 (1994).

[5] J. H. Xiao, G. Hu and Z. Qu, Phys. Rev. Lett. **77**, 4162 (1996); Y. Zhang, G. Hu and L. Gammaitoni, Phys. Rev. E **58**, 2952 (1998); M. Hasler, Int. J. Bifurcation Chaos Appl. Sci. Eng. **8**, 647 (1998).

[6] B. P. Bezruchko, V. Yu. Gulyaev, S. P. Kuznetsov and E. P. Seleznev, Dokl. Akad. Nauk (SSSR) **287**, 619 (1986) [Sov. Phys. Dokl. **31**, 268 (1986)]; A. P. Kuznetsov, S. P. Kuznetsov and I. R. Sataev, Int. J. Bifurcation Chaos Appl. Sci. Eng. **1**, 839 (1991).

[7] S.-Y. Kim, Phys. Rev. E **59**, 6585 (1999); S.-Y. Kim and W. Lim, Phys. Rev. E **63**, 036223 (2001); S.-Y. Kim, W. Lim and Y. Kim, Prog. Theor. Phys. **106**, 17-37 (2001); Y. Kim, J. Korean Phys. Soc. **44**, 506 (2004).

[8] A. P. Kuznetsov, S. P. Kuznetsov and I. R. Sataev, Int. J. Bifurcation Chaos Appl. Sci. Eng. **3**, 139 (1993).

[9] B. Derrida, A. Gervois and Y. Pomeau, J. Phys. A **12**, 269 (1979); B. Derrida and Y. Pomeau, Phys. Lett. A **80**, 217 (1980); B. Hu and J. M. Mao, Phys. Rev. A **25**, 1196 (1982); **25**, 3259 (1982); Phys. Lett. A **108**, 305 (1985); J. M. Mao and R. H. G. Helleman, Phys. Rev. A **35**, 1847 (1987); S.-Y. Kim, J. Korean Phys. Soc. **22**, 406 (1989); S.-Y. Kim and B. Hu, Phys. Rev. A **41**, 5431 (1990).

[10] M. Schell, S. Fraser and R. Kapral, Phys. Rev. A **28**, 373 (1983).